Tenth International Conference on Computational Fluid Dynamics (ICCFD10), Barcelona,Spain, July 9-13, 2018

ICCFD10-120

Influence of evaporation models on a lift-off height of a spray jet flame

J. Stempka*, L. Kuban* and A. Tyliszczak*
Corresponding author: stempka@imc.pcz.pl

* Institute of Thermal Machinery, Czestochowa University of Technology,
Faculty of Mechanical Engineering and Computer Science,
Armii Krajowej 21, 42-201 Czestochowa, Poland

Abstract: In the current work the jet spray combustion process, reflecting an experimental configuration of a piloted spray burner with a vitiated co-flow is simulated numerically. In the simulation a diluted ethanol spray evaporates in the hot surrounding, then the gaseous fuel diffuses from spray fuel-rich core into the oxidizer fuel-lean region and auto-ignites. An in-house high-order compact difference LES solver is used to carry out the computations. The reaction rates are computed using Implicit LES approach along with a single-step chemical global reaction. The continuous phase is modelled in the Eulerian reference frame while the droplets in the Lagrangian form. We analyse an influence of evaporation models on the flame lift-off height, flame spread and its characteristics. Results show relatively good agreement with experimental measurements of lift-off heights predictions regardless of the evaporation model used. However, the flame statistics, e.g., temperatures and fuel distribution significantly differ from model to model. The key parameter of evaporation models influencing slightly the results is the evaporation rate. It was showed that ILES is able to correctly represent qualitative flame features.

Keywords: LES, turbulent combustion, evaporation models, two-phase flows.

1 Introduction

The combustion processes are one of the most fundamental ways of global energy conversion. A variety of industrial and small scale devices operate being powered as a consequence of highly turbulent combustion processes that follow the the liquid fuel injection, e.g., diesel engines, liquid powered burners, aircraft propulsion systems, liquid fueled rockets engines and many others. Therefore studies of reacting two-phase flows involving the diluted fuel sprays in gaseous carrier medium, constitute a very important research field in flow dynamics. Recent advances in combustion science have lead to the development of more efficient and less pollutant ways of fuels utilization (e.g., fuel-lean operation, reheat systems).

Experimental [1, 2] and numerical [3, 4] studies of combustion of gaseous fuels are very advanced by now. There is a variety of numerical methods for simulating turbulent gaseous flames, i.e., performed via direct numerical simulations (DNS), large eddy simulations (LES) and Reynolds-averaged numerical simulations (RANS). In opposition to the research of gaseous fuels the sprays combustion still shows as an open field for advancements in both experimental and numerical aspects. Even though, many studies emerged in the past, due to high complexity of such a flows they are mostly limited to fundamental cases. In the realistic regimes prior to the formation of combustible mixture the injected stream of fuel is subjected to various physical processes, e.g., droplets dispersion and evaporation, mixing of fuel vapour, occurrence of chemical reactions. The difficulties of turbulent spray combustion analysis arises from a range of interlinked phenomena that cannot be fully captured by the experiment. Hence, new numerical studies emerge using both the DNS [5] and LES [6] approaches. On the one hand, the DNS provides a detailed insight to the turbulent and reacting

two-phase flows nature but on the other hand is limited mainly to flows in simplified domains and assuming low Reynolds numbers. Thus the LES boost further advancements in spray combustion research.

In the framework of LES, the biggest challenge in simulations of turbulent flames constitutes a proper way of capturing the turbulence-flame interactions at sub-grid level influencing the reaction rates. Various strategies for modelling the reaction rates can be employed, such as: Lagrangian Particles, transported PDFs, Eulerian stochastic fields along with Monte Carlo solution techniques. There are also simpler modelling methods, promising from practical point of view, i.e., implicit LES (ILES) [7]. The ILES method is particularly well suited for comparative and parametric studies of complicated reacting flows as it is robust and provides fairly reliable solutions. Another issue of an appropriate simulations is the modelling of evaporation processes. Most popular are the evaporation models based on the simplified assumptions but allowing the problem to be tractable practically. Various evaporation models are adopted in analyses and these can be listed in growing complexity level as: infinite conductivity models, finite conductivity models, non-equilibrium models and also rather rare full solutions of Navier-Stokes equation of evaporating droplets. The preceding one is obviously beyond the practical interest but the remaining ones are promising and already thoroughly used. Hence, we decided to compare their capabilities in predicting evaporation rates, enthalpy fluxes and to asses to which extent they may influence the flame characteristics. In the current work we compare results obtained using: (i) "D^2 law" [8, 9], (ii) infinite conductivity model incorporating Stefan flow effect [10] and (iii) infinite conductivity non-equilibrium evaporation model based on a Langmuir-Knudsen law [11, 12].

In any event, the experimental studies on turbulent multiphase flames are essential for validating the numerical methods. Fortunately, with the advent of new measurement techniques, more detailed results are now obtainable. A great example is the experimental research done by the group of Professor's Masri form Sydney University. Authors provided a comprehensive database that are specifically intended for numerics validation purposes because of variety of data they captured and suitable prescription of boundary conditions essential in numerical studies. The work covers range of different setups of experimental vitiated co-flow piloted spray burner assembly for which different kind of nozzles, co-flows temperatures and fuels were tested. As a reference for current studies we chose the experimental burner setup according to work of O'Loughlin et al. [1]. Authors provide a comprehensive experimental study which include Phase Doppler Anemometry (PDA), Laser Doppler Velocimetry (LDV) and temperature measurements. The results were used to build a database which comprises the fuel fluxes, temperatures and velocity profiles measurements to which we will refer.

In the current analysis the autoignitig jet flame, fed by the fuel (ethanol) spray within the vitiated co-flow is investigated numerically. The computational domain along with prescribed boundary conditions mimic the experimental burner examined formerly by O'Loughlin et al. The process involved in the burner operation include droplets evaporation in the hot surroundings, diffusion of gaseous fuel from spray fuel-rich core into the oxidizer fuel-lean region and eventually autoignition. Our studies are mainly focused on the question how the flame is affected by the numerical models. The main goal of the current research is to asses the validity of LES applied to turbulent two-phase flames. The next objective is to compare different evaporation models performance in predicting the flame characteristics with regards to the experimental results. We are particularly interested in investigation of an impact of the spray evaporation model on the resulting lift-off height. The applied models take into account convective and blowing effects with various correlations for Nusselt and Sherwood numbers. For the current comparative study only the evaporation model is changed keeping the same initial setup for each case. An in-house numerical solver SAILOR [13] is used to carry out the computations. The continuous phase flow is calculated in Eulerian reference frame whereas the discrete phase is transported in the flow field in Lagrangian coordinates. A global mechanism is applied for chemistry along with the reaction rate that is calculated based on filtered values. Such a strategy is found to be sufficient for the current comparative study, since the accuracy of the lift-off height predictions is only slightly affected by the chemical mechanism [14]. Finally, an assessment of the impact of the spray evaporation model on the jet flame lift-off height is provided. Statistical and graphical results are presented and discussed in details.

2 Mathematical model

We consider a low Mach number reacting flow which is simulated by solving the LES set of transport equations. These are obtained by applying the spatial filtering and Favre averaging procedure to the Navier-Stokes equations. The filtering procedure is defined as:

$$\bar{f}(\mathbf{x}) = \int G(\mathbf{x} - \mathbf{x}^{'}, \Delta(\mathbf{x})) f(\mathbf{x}^{'}, t) \mathbf{dx}^{'} \tag{1}$$

where G is the filter function and $\Delta(\mathbf{x})$ is the filter width. For capturing the large density variations in reacting flow the Favre-averaging operation is applied as:

$$\tilde{f}(\mathbf{x}, t) = \frac{\overline{\rho(\mathbf{x}, t) f(\mathbf{x}, t)}}{\bar{\rho}(\mathbf{x}, t)} \tag{2}$$

Application of the above procedures lead to the following set of LES governing equations, i.e., continuity and momentum:

$$\frac{\partial \bar{\rho}}{\partial t} + \frac{\partial \bar{\rho} \tilde{u}_j}{\partial x_j} = \bar{\dot{S}}_{mass} \tag{3}$$

$$\frac{\partial \bar{\rho} \tilde{u}_i}{\partial t} + \frac{\partial \bar{\rho} \tilde{u}_i \tilde{u}_j}{\partial x_j} = -\frac{\partial \bar{p}}{\partial x_i} + \frac{\partial \bar{\sigma}_{ij}}{\partial x_j} + \frac{\partial \tau_{ij}^{sgs}}{\partial x_j} + \bar{\dot{S}}_m \tag{4}$$

where the $\bar{\sigma}_{ij}$ denotes the viscous stress tensor and $\tau_{ij}^{sgs} \equiv \bar{\rho} \widetilde{u_i u_j} - \bar{\rho} \tilde{u}_i \tilde{u}_j$ is a trace-free part of the sub-grid stress tensor. Only the deviatronic part of the τ_{ij}^{sgs} is relevant since the gradient of its trace is absorbed into the effective pressure field. It is modelled using eddy-viscosity closure of a generic form $\tau_{ij}^{sgs} - 1/3 \delta_{ij} \tau_{kk} = -2\mu_{sgs} \tilde{S}_{ij}$ where $\tilde{S}_{ij} = 1/2(\partial \tilde{u}_j / \partial x_i + \partial \tilde{u}_i / \partial x_j)$ is the resolved strain rate tensor. The sub-grid scale eddy viscosity μ_{sgs} is calculated using the Vreman model [15].

The species mass fraction ($\tilde{\phi}_\alpha$) and the enthalpy (h) transport equations are given as, respectively:

$$\frac{\partial \bar{\rho} \tilde{\phi}_\alpha}{\partial t} + \frac{\partial \bar{\rho} \tilde{\phi}_\alpha \tilde{u_j}}{\partial x_j} = \frac{\partial}{\partial x_j} \left[\left(\frac{\mu}{\sigma} + \frac{\mu_{sgs}}{\sigma_{sgs}} \right) \frac{\partial \tilde{\phi}_\alpha}{\partial x_j} \right] + \bar{\dot{S}}_\alpha + \overline{\rho \dot{\omega} (\phi_\alpha)} \tag{5}$$

$$\frac{\partial \bar{\rho} \tilde{h}}{\partial t} + \frac{\partial \bar{\rho} \tilde{h} \tilde{u_j}}{\partial x_j} = \frac{\partial}{\partial x_j} \left[\left(\frac{\mu}{\sigma} + \frac{\mu_{sgs}}{\sigma_{sgs}} \right) \frac{\partial \tilde{h}}{\partial x_j} \right] + \bar{\dot{S}}_h \tag{6}$$

in which the μ and σ represent the molecular viscosity and Prandtl/Schmidt number. The unknown sub-grid scale contributions in above equations resulting from the filtering procedure are modelled with the Schmidt and Schumann model [16] which incorporates the sub-grid Prandtl/Schmidt number σ_{sgs}. Currently it is also assumed that the ratio of the thermal to mass diffusivities are the same, i.e., the Lewis number is equal to unity. The term $\overline{\rho \dot{\omega} (\phi_\alpha)}$ denotes the reaction rate.

2.1 Source terms

The dispersed phase is coupled with the flow field through the source terms appearing in Eqs. (3) to (6). They represent averaged sums of the contributions from all particles at each computational cell. Generally, one may write $\bar{\dot{S}} = 1/\Delta^3 \sum_{p=1}^{N_p} \dot{S}_p$ where the Δ and p refer to the spatial filter width and p-th droplet, respectively. The subscripts f and d denote the fuel liquid phase and the droplet. The source terms are expressed as:

$$\bar{\dot{S}}_{mass,p} = \bar{\dot{S}}_{\alpha,p} = -\frac{d}{dt} m_{d,p} \tag{7}$$

$$\bar{\dot{S}}_{m,p} = -\frac{d}{dt} \left(m_d v_d \right)_p \tag{8}$$

$$\bar{\dot{S}}_{h,p} = -\left(c_f m_d \frac{T - T_d}{\tau_d^T} + \frac{dm_d}{dt} h_f \right)_p \tag{9}$$

where T denotes the resolved flow temperature interpolated at the droplet position, c_f is specific heat capacity and τ_d^T is the relaxation time:

$$\tau_d^T = \frac{\rho_f D_d^2}{6Sh} \frac{PrLe}{\mu_f} \frac{B_T}{ln(1+B_M)} \frac{C_f}{C_{f,v}} \tag{10}$$

where ρ_f is the liquid fuel density, D_p is the particle diameter, Pr, Sh and Le are the Prandtl, Sherwood and fuel Lewis numbers, respectively. B_T is the temperature Spalding number, $C_{f,v}$ and μ_f are the fuel vapour heat capacity and the dynamic viscosity of the fuel.

2.1.1 Dispersed phase

Dispersed phase motion is described in Lagrangian coordinates. The model is drawn from the work of Maxey and Riley [17], except the stochastic term for modelling the sub-grid contribution on the spray motion, which is not taken into account. The equations of the droplets motion are given as:

$$\frac{dx_d}{dt} = v_d \tag{11}$$

$$\frac{dv_d}{dt} = \frac{\tilde{u} - v_d}{\tau_d^v} \tag{12}$$

where $\tilde{u}$ is the gas phase velocity at the droplet's position and the particle relaxation time τ_d^v is expressed as:

$$(\tau_d^v)^{-1} = \frac{3}{8} \frac{\rho_f}{\bar{\rho}} C_D \frac{|\bar{u} - v|}{r_d} \tag{13}$$

the C_D is the drag coefficient from correlation [18] and r_d is the droplet radius.

2.1.2 Evaporation model

The droplets are treated as point sources of mass, momentum and enthalpy. Instantaneous changes in droplet mass and temperature are calculated by integrating the set differential equations consistently with the Miller et al. [11] formulation:

$$\frac{dT_d}{dt} = \frac{f_2}{3} \frac{Nu}{Pr} \left(\frac{\theta}{\tau_d} \right) (T - T_d) + \left(\frac{h_f}{c_f} \right) \frac{\dot{m}_d}{m_d} \tag{14}$$

$$\frac{dm_d}{dt} = -\frac{Sh}{3Sc} \left(\frac{m_d}{\tau_d} \right) H_M \tag{15}$$

the formulation incorporates following terms: $\theta = c_{p,g}/c_f$ is the fuel vapour-gas mixture to the liquid fuel heat capacities ratio, $\tau_d = \rho_f D^2/18/\mu_g$ is a relaxation time. The correction coefficient and the mass transfer potential are denoted by f_2 and H_M, respectively (see tab. 1). The dimensionless numbers (Prandtl, Schmidt, Nusselt and Sherwood) are computed as $Pr = \mu_g c_{p,g}/\lambda_g$, $Sc = \mu_g/\rho_g \Gamma_g$. For the Nu and Sh numbers appropriate correlations for non-stationary droplets given by Clift et al. [19] are used, while for Nu and for Sh, the correlations suggested by Abramzon and Sirignano [10]. In above definitions, terms: Γ_g, λ_g and μ_g represent binary diffusion coefficient calculated from Hirschfelder equation [20], thermal conductivity and fuel vapour-gas mixture dynamic viscosity. The term $\dot{m}_d = dm_d/dt$ defines the rate of change droplet mass. The physical parameters denoted by the subscript g are calculated adopting the "1/3 rule" [18] of mixing expressed as:

$$T_R = T_d + 1/3\,(T - T_d) \tag{16}$$

$$\phi_R = \phi_d + 1/3\,(\phi_\alpha - \phi_d) \tag{17}$$

The above quantities are obtained in the reference temperature T_R and mass fraction ϕ_R, respectively. By adopting the mixing rules the averaged physical quantities become dependent on spatial and thermal variations of flow variables thus gaining the physical consistency.

In the current work, three different evaporation models were variably applied for calculations. These are the "D^2 law" [8, 9] (E1), infinite conductivity model incorporating Stefan flow effect [10] (E2) and infinite

conductivity non-equilibrium evaporation model based on a Langmuir-Knudsen law [11, 12] (E3). Details of each model parameters are summarised in tab. 1. In which $B_{M,eq}$ and $B_{M,neq}$ denote equilibrium and non-equilibrium Spalding transfer numbers. Both are defined as the ratio of the difference of the fuel vapour mass fraction at the droplet film and away from the droplet to the mass fraction of a carrier medium at the droplet surface.

Table 1: Evaporation models parameters

Model	f_2	H_M
E1	1	$ln\left(1+B_{M,eq}\right)$
E2	1	$B_{M,eq}$
E3	G	$ln\left(1+B_{M,neq}\right)$

In non-equilibrium model the fuel content at the droplet surface is calculated using the modified mole fraction formula: $\chi_{s,neq} = \chi_{s,eq} - 2\beta L_K/D$, where $\chi_{s,neq}$ is calculated using Clausius-Clapeyron equation, L_K is the Knudsen layer thickness and $\beta = -\left(\frac{3Pr\tau_d}{2}\frac{\dot{m}_d}{m_d}\right)$ is the model parameter. Finally, the G term is related to β parameter by $G = \beta/\left(e^{\beta}-1\right)$. Obviously, the non-equilibrium effects are accounted by introducing an additional parameter into equilibrium mole fraction term. Note that when $\lim_{\beta\to 0} G = 1$, for example if droplet does not evaporate, E3 converts to E1.

2.1.3 Reaction rate

The Implicit LES (ILES) approach [7] is employed to compute the $\overline{\dot{\omega}\left(\phi_\alpha\right)}$. The main difference between LES and ILES relies on treatment of the reaction source terms. In ILES similarly to LES the sub-filter scales resulting from the filtration of the convective terms are modelled by eddy-viscosity model, but in ILES the chemical source terms $\overline{\dot{\omega}(\phi_\alpha)}$ are modelled assuming $\overline{\dot{\omega}(\phi_\alpha)} \approx \dot{\omega}(\tilde{\phi_\alpha})$ [7]. In the current analysis reaction rates are obtained from the Arrhenius formula using one-step global chemistry following the ethanol oxidation reaction:

$$C_2H_5OH + 3(O_2 + 3.76N_2) = 2CO_2 + 3H_2O + 3\cdot 3.76N_2 \tag{18}$$

for which the reaction rate is tuned to give a reasonable prediction of the strain rate extinction [21]. This approach was chosen to reasonably minimize the computational expense and to asses potential discrepancies which simplified modelling of the reaction term can bring into the results. Even though estimation of the reaction rates based on filtered values is known from over-predicting the flame speed for rich mixtures as discussed in [22] yet it still can reproduce correct trends in the analysis of turbulence impact on the ignition and flame propagation without resolving the flame speed at all equivalence ratio range in details. The ILES assumption would certainly fail in the Reynolds Averaged Navier-Stokes (RANS) framework as the fluctuations in RANS models are large. On the other hand the ILES is valid for laminar flow simulations and in DNS where all turbulent flow scales are resolved. Hence, one may assume that for sufficiently dense computational meshes, when the grid cells are comparable with the Kolmogorov length scale, the ILES approach can be appropriate.

3 Configuration

In the work we focus on modelling the vitiated co-flow piloted jet spray burner configuration similar to the one studied by O'Loughlin et al. [1]. The burner configuration is presented in Fig. 1. The burner assembly along with measurement rig was developed by the Professor Assaad Masri's group at the University of Sydney. The burner consists of an ultrasonic nebulizer device which generates spray with specific Sauter mean diameter (SMD) (currently about 40 μm) at the inlet of the central jet nozzle with a diameter of $d_j = 4.6\ mm$. The generated spray at zero initial velocity is carried downstream the central tube by the co-flowing stream of air. Around the central nozzle the annular co-flow assembly is assembled. The diameter

of the co-flow assembly is equal to 197 mm and it is terminated by the perforated plate with 2200 holes, each with a diameter of 1.58 mm. The perforated plate is placed 68 mm upstream of the exit plane of the jet nozzle. During operation the lean (equivalence ratio $\phi = 0.38$) hydrogen/air flame with a temperature of $T_c = 1380\ K$ is issued from each of the hole at the perforated plane with the velocity which is equal to 3.5 m/s. The whole burner assembly is placed in the wind tunnel to shroud the co-flow.

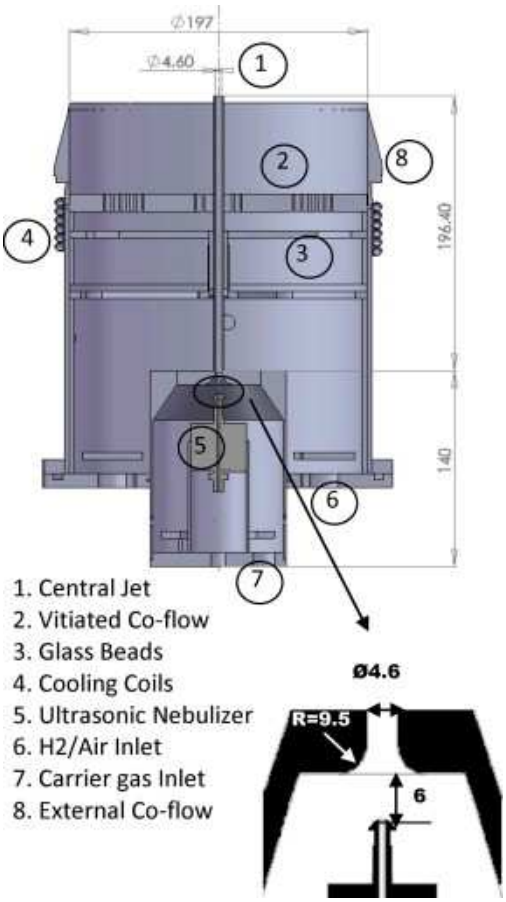

Figure 1: Experimental burner assembly [1].

From the experiment the data from several spray flames are available because different fuels, mass loadings and co-flow temperatures were tested. The measurements done during the study include: Laser Doppler Velocimetry for the mean and RMS velocity fluctuations, Phase Doppler Anemometry for droplet fluxes and size distribution, planar imaging for selected species and temperature measurements by using thermocouples with wire thickness of 0.15 mm. In the current study we chose well documented results from ethanol spray flame (Et1A) experiment. The jet of spray was issued from the jet nozzle with a bulk velocity of $U_j = 75\ m/s$ and burned in the hot co-flow.

The simulation domain comprises a rectangular volume segment of the burner aligned with the jet axis. It starts at the jet exit plane and terminates $50d_j$ downstream. The other dimensions of the domain are equal to $15d_j$. The domain is discretised by $240 \times 160 \times 160$ nodes and the resulted computational mesh is presented in Fig. 2 along with the prescription of the main characteristic of an analyzed setup. The mesh is compressed at the vicinity of the exit plane and along the jet, i.e., in the region where high scalar gradients are expected. Resulting mesh spacing are as follow: $\Delta x = 1.2 \cdot 10^{-4} \div 1.2 \cdot 10^{-3}$, $\Delta y = 2.7 \cdot 10^{-4} \div 2.2 \cdot 10^{-3}$, $\Delta z = 1.2 \cdot 10^{-4} \div 1.2 \cdot 10^{-3}$. Boundary conditions applied in the simulations anywhere except the inlet and outlet are characterised by the Neumann boundary condition with zero gradient. At the outlet the outflow boundary condition is prescribed. While the the inlet the velocity profile is imposed, according to the experimental profile LDV measurements at the exit plane. Since the mixture fraction profile at the inlet

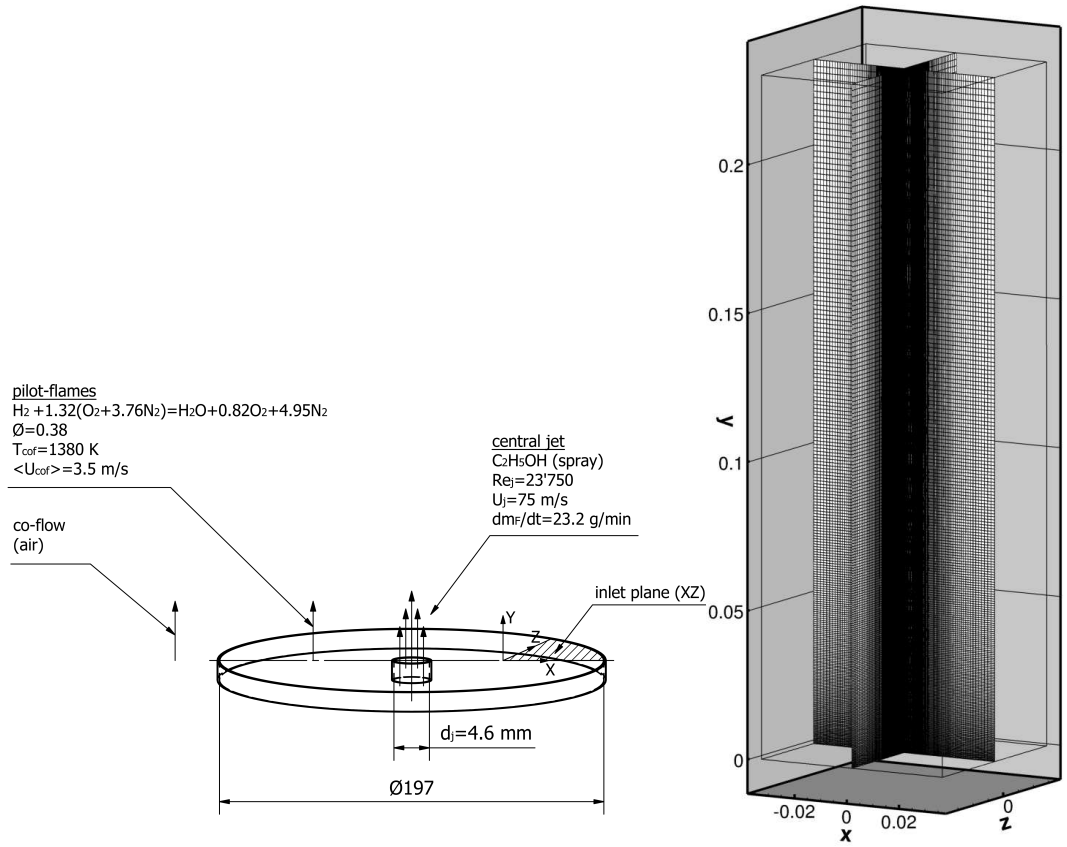

Figure 2: Inset on the inlet plane (left) and computational mesh (right).

was not available from the experiments we assumed it be uniform across the jet nozzle. Anywhere outside the jet inlet region the hot co-flow of lean air/hydrogen combustion products with temperature and velocity corresponding to the experiment are assumed.

Instead of reproducing the exact droplet distribution issuing at multiple points from the jet nozzle, we applied simplified approach for computational savings. The spray in simulations is injected from random point, which at each time step obtains different location placed in the region of the jet nozzle outlet. We defined 10 classes of droplets diameters with $SMD = 40\ \mu m$. The resulting fuel mass flow of liquid droplets is kept the same as in the experiment, i.e., 23.2 g/min. The droplets similarly as the carrying air stream, initially have the room temperature. The simulation is carried out with the variable time step for which the Courant-Friedrichs-Lewy condition is set to 0.2.

4 Numerical procedure

Computations were carried out using an in-house academic LES solver SAILOR [13]. The code solves a low Mach number approximated set of equations, disregarding acoustics modes. The derivatives in Navier-Stokes and energy equations are discretised in Cartesian coordinates on collocated grid arrangement and half-staggered mesh for the pressures nodes. Derivatives are formulated based on a high-order compact difference scheme [23]. The staggered grid arrangement ensures oscillation-free pressure field since the pressure nodes are decoupled from values stored in collocated grid. Staggered pressure nodes require implementation of the interpolation procedure and currently the interpolation up to 10^{th} order is used for both, the interpolation and derivative approximations. The pressure field is resolved using pressure correction and calculated from Poisson equation. It is formulated based on a continuity equation with interpolated derivatives and corrected mass fluxes. Each of the transport equation is discretised using the compact difference scheme except the

convective terms in species equations. Currently the 5^{th} order Weighted Essentially Non-Oscillatory scheme is used for the convective terms in species equation discretisation. The governing equations are integrated in time with the use of predictor-corrector approach. At the predictor step, the second order Adams-Bashforth method is used and at the corrector step the second order Adams-Moulton method. For solving equations that govern the dispersed phase motion, we applied 1^{st} order integration. The two-way velocity and temperature coupling is performed using 2^{nd} order approximation of momentum source terms with 4^{th} degree Lagrangian polynomial approximation of the flow field velocity at the droplets positions. The numerical code was thoroughly tested and validated for various configurations including both non-reacting and reacting flows [4, 24, 25, 26].

5 Results

5.1 Lift-off heights

O'Loughlin et al. [1] performed a detailed study of lift-off heights (L_h) for several flame conditions. Figure 3 shows a direct comparison of the mean temperature fields obtained for different evaporation models (labeled as E1, E1 and E3) with experimental data of O'Loughlin et al. [1]. Clearly the lift-off heights predicted in computations correspond well to the experimental data. The last sub-figure presents a photography of an experimental flame where appropriate measure scale are given convenience. The lift-off height reported in the [1] for the (Et1A) flame was equal to $L_h \approx 15$. This indicates good agreement with E2 model and only small underprediction of models E1 and E3 are observed.

The results reveal only small differences between flames lift-of heights predicted by the different models. Concerning only the upstream tip of the high temperature region, the evaporation models E1 and E3 agree

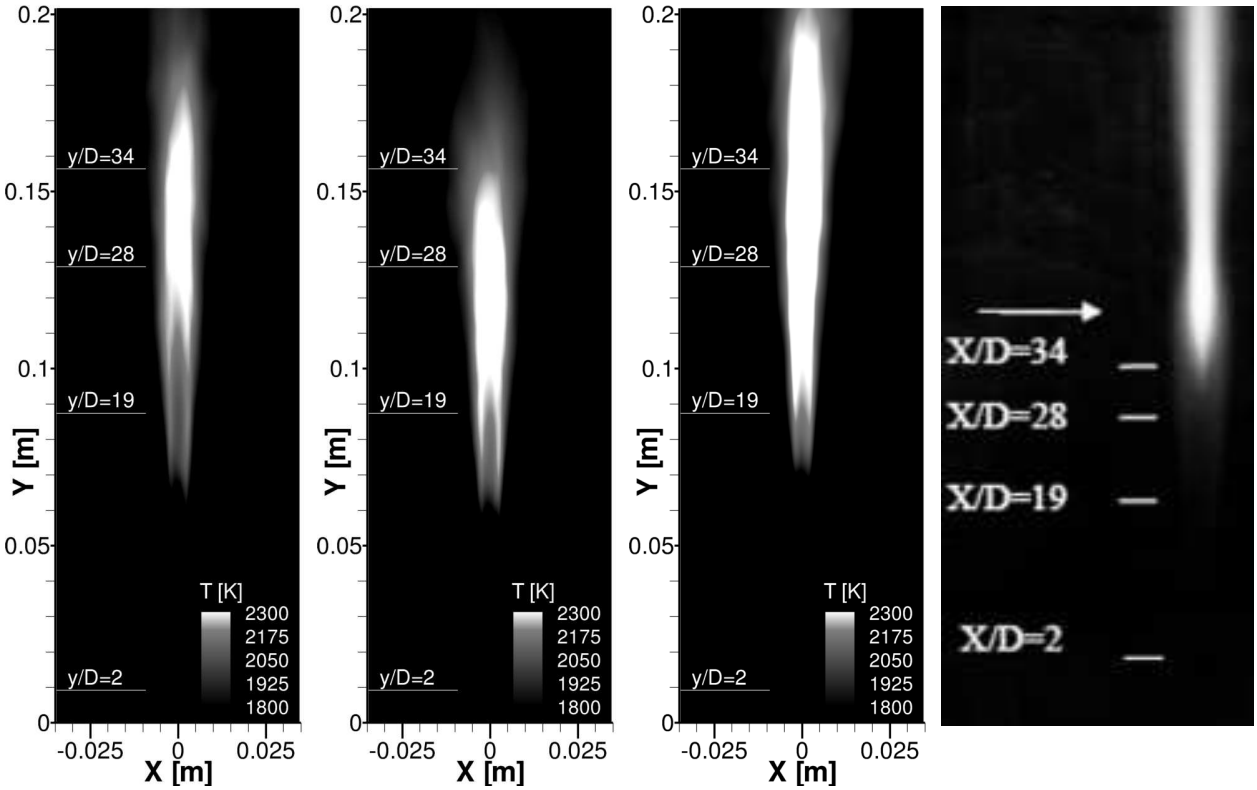

(a) Model E1 (b) Model E2 (c) Model E3 (d) Experimental

Figure 3: Averaged temperatures distributions obtained using models: E1, E2 and E3 vs. experimental flame.

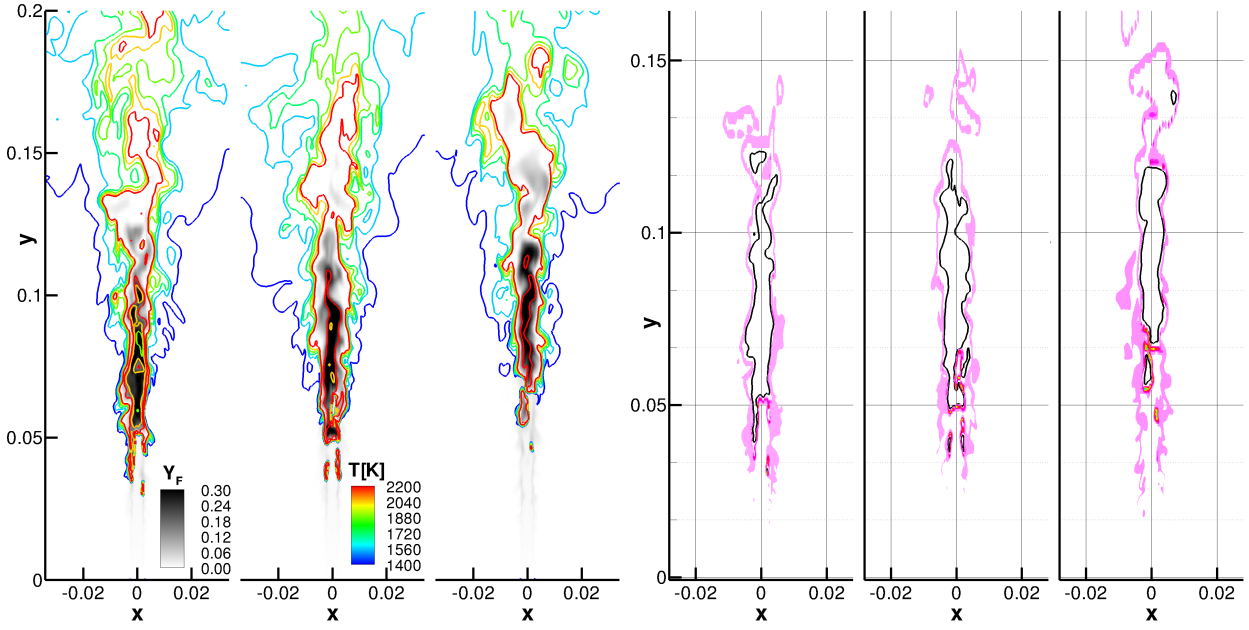

Figure 4: Instantaneous distributions of: a) temperatures (iso-lines) and fuel mass fraction (fields) and b) heat release (pink) with stoichiometric fuel mass fraction iso-line.

with the experimental measurements quite well. In case of use of the E2 model a slight underprediction of the lift-of height $L_h \approx 13$ is evident. Such underprediction may be due to the slightly higher evaporation rates predicted by the model E2. It can be viewed as a model that results in more intensive evaporation comparing to models E1 and E3. This feature is more likely attributed to differences in H_M terms defining each model, i.e., in E1 $H_M = ln(1 + B_M)$ while in E2 $H_M = ln(1 + B_M)$. Thus noting that $dm/dt \propto H_M$ it results in conclusion that evaporation rate is always higher when logarithm function is omitted. The high temperature region is elongated mostly for the model E3, indicating the complex behaviour of non-equilibrium model predictions. It was found by others that the non-equilibrium effects enhance mostly the evaporation rates of smaller droplets (less than 50 μm), by significant fuel contribution to the surface mole fraction [27]. Additionally, the differences between the models can be seen analysing the distance of spray penetration into the hot reaction zone. This distance is found to be the highest for the flame simulated with the model E1 which seems to be in best agreement with the experimental data.

Figure 4 presents the instantaneous distributions of temperature along with the fuel mass fraction 4 a) and the heat release distributions for each evaporation model 4 b). The instantaneous contours of temperature and heat release reveal that the reactions occur at a broad range of the fuel mass fractions. It is evident that high temperature reaction zone slides upstream the spray jet. This is due to the fact that some amount of fuel that evaporated initially from the spray core, mixes intensively with the oxidizer within the mixing layer which developed from the nozzle exit. The pockets of high heat release which forerun the autoignition are moved even more upstream and correspond to the lean fuel regions. However, due to insufficient temperature as it is lowered by the heat diffusion from the hot co-flow into the spray core, the mixture ignites further downstream.

These high heat release regions are aligned with the fuel mass fractions slightly below stoichiometric. Therefore, the differences in fuel content in that region have detrimental effect on the autoignition axial spots. It is also noticeable that the model E2 resulted in prediction of appearance of the stoichiometric conditions slightly early compared to the remaining models, which in turn led underprediction of the L_h.

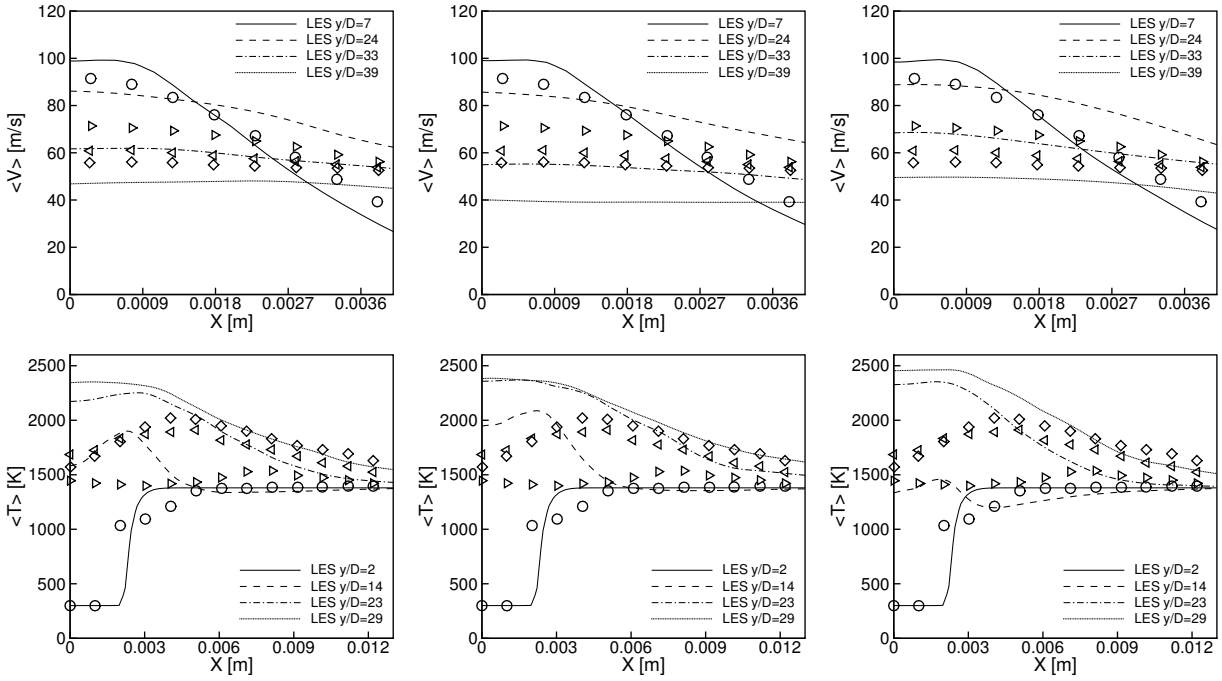

(a) Model E1 (b) Model E2 (c) Model E3

Figure 5: Statistics presenting $\langle V \rangle$ and $\langle T \rangle$ obtained using models: E1, E2 and E3 vs. experimental data. Symbols denote experimental data from jet sections at: ($\circ$) y/D=2, ($\triangleright$) y/D=19, ($\triangleleft$) y/D=28 and ($\diamond$) y/D=34.

5.2 Temperature and velocity statistics

The plots in Fig. 5 show distributions of the quantities measured experimentally along the sections perpendicular to the jet axis at axial distances equal to y/D=2, y/D=19, y/D=28 and y/D=34 denoted by the symbols. The profiles of mean temperature and axial velocity obtained using different evaporation models are presented by the lines. The overprediction of temperature in the reaction zone influenced the velocity profile also by the high density variations. Therefore, instead of analysing the exact same locations which were attributed to significant discrepancies in simulations we present the data for shifted sections that correspond to experiment most accurately.

It can be seen from the first row of the presented results that slight shift of the measuring section, along the jet axis gives reasonable agreement for the velocity profile placed close to the jet exit plane (up to the y/D=24). No significant differences in impact of the evaporation model can be observed for the velocity profiles. The discrepancies are clearly present for downstream sections, which are probably the most pronounced in case of the model E2. Further inspection of the temperature profiles reveals that for measuring sections placed below the experimental ones, the profiles show overprediction of temperatures in the jet core region. However, the discrepancies diminish radially. It can be observed that the overprediction of temperatures lead to the significant drop of density in the spray core early upstream. Thus, affecting the velocity field for which the velocity peaks in high temperature regions were highly over-predicted. The characteristic depression of the temperatures profile at the jet axis is not reproduced by the simulation. This issue is believed to be attributed to the use simple one-step global chemistry mechanism or simplified reaction rate modelling. However, concerning the main goal of the current studies this inefficiencies are not regarded to false the final output from the work. Generally, the flame characteristics were found to be affected by the evaporation model rather slightly, similar observation for the hollow cone burner was also made by other researchers [27].

5.3 Spatial resolution

In the ILES approach for sufficiently dense meshes values resulting from the spatial averaging approximate spatial variations of the flames very well. Therefore it is interesting to look for the source of potential discrepancies in spatial resolution relative to the local flow structures. To asses the LES quality we provide the results of the axial variations of the ratio of mesh characteristic size to the flow characteristic sizes (Fig. 6). The analysis is based on calculated integral length scale l_0 and Kolmogorov length scale η_K. In

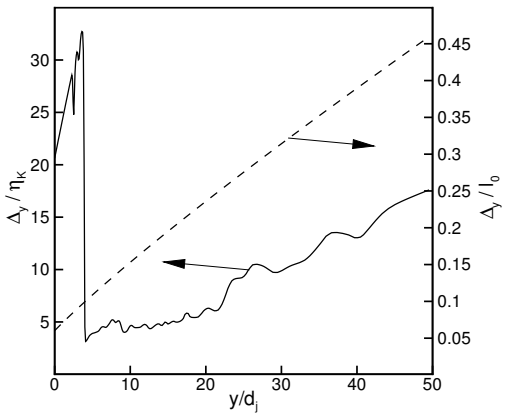

Figure 6: Axial variations of the grid resolution in the simulations with respect to the characteristic flow scales.

a round jet, the integral length scale can be approximated by $l_0 \approx d_j\,(1 + B \cdot z)$ where $B \approx 0.09$ is the expansion rate of the jet [28]. Having the l_0 we estimate the Kolmogorov length scale as $\eta_K = l_0 Re_L^{-3/4}$, for which $Re_L = u' l_0/\nu$ where the RMS of velocity u' is calculated as an ensemble average from results after the statistically steady state was reached by the jet. The analysis of the ratio of the characteristic mesh spacings in the axial direction Δ_y across the whole domain shows that spacings between grid points were less than 45% of the l_0 and less than 35% of the l_0 along the domain. At the same time the grid was no greater than about $20\eta_K$ in most part of the domain. It seems that the used grid can be regarded as rather fine for LES simulations, however, the grid test is left for the further studies.

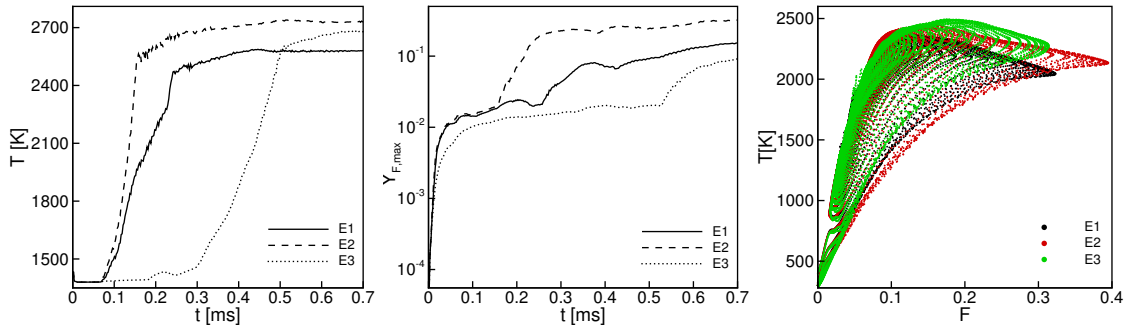

(a) (b) (c)

Figure 7: Comparison of the evaporation model impact presented by: a) plot of maximal temperature time variations inside the domain, b) plot of maximal mass fraction values over time variations, c) scatter plots of temperatures in the mixture fraction space.

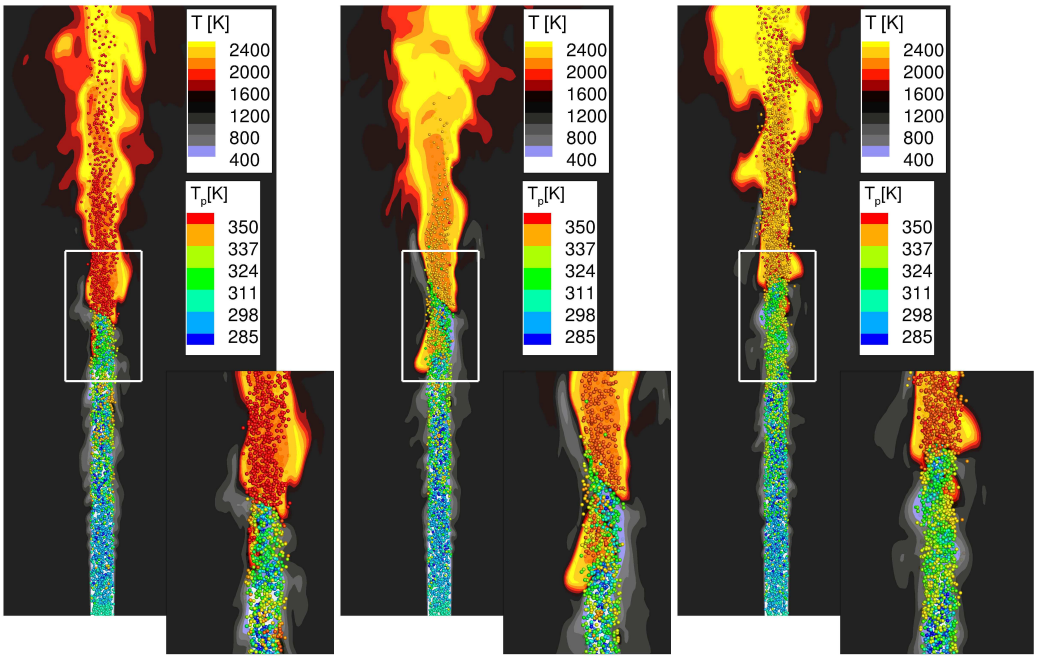

(a) Model E1 (b) Model E2 (c) Model E3

Figure 8: Instantaneous planar temperatures distributions, with droplet coloured by the drops' temperatures and scaled by their diameters. Inset on the tip of reaction zone.

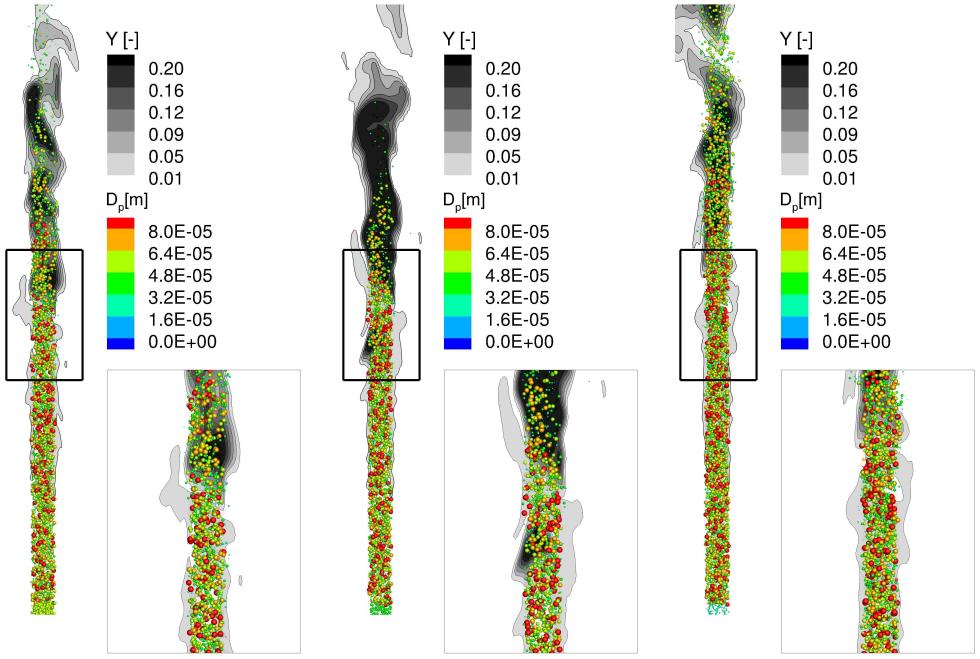

(a) Model E1 (b) Model E2 (c) Model E3

Figure 9: Instantaneous planar fuel distributions, with droplet coloured and scaled by the drops' diameters. Inset on the tip of reaction zone.

5.4 Model comparison

The current section is devoted to analysis of the differences between the evaporation models influence on spray and other aspects of the flow in greater detail. The autoignition delays for each of the evaporation model applied in the computations are presented in fig. 7 a). It clearly displays significant delay in autoignition time predicted by the model E3. The delays is considerable respectively to the models E1 and E2. The reason for such effect is further investigated through the analysis the plot of instantaneous values of the fuel content growth showed in fig. 7 b). It is evident that indeed in case of the model E3 the fuel content growth was slower than corresponding growth for E1 and E2 models. This effect could be attributed to the non-equilibrium effect which seems that before reaction and entrance in high temperature region, have negligible effect in enhancing small droplet evaporation.

Additionally the scatter plot of the mean temperatures measured inside the domain in the mixture fraction space is given in Fig. 7 c). The colors of the scatters correspond to different evaporation models. Here one may observe that each of the evaporation models have different impact on the maximal temperatures obtained in the domain. They also differ in the range of mixture fraction for which high temperature appear. For example, use of model E1 resulted in lowest maximal temperature reached in the domain while for the model E3 maximal temperatures were slightly higher comparing to other models. The reason can be related to the lower evaporation rates predicted by the model E3 indicating that the droplet heating was not very rapid and hence generally the spray influenced less the temperatures in the reaction zone. The feature of the model E3 is the lowest scatter of the temperatures in the mixture fraction space among the applied models. The implementation of the model E2 resulted in significantly higher range of mixture fraction for which combustion takes place is comparing to the remaining two models. The reason may be, again, attributed to higher evaporation rates for model E2 which accumulates locally the higher fuel content prior to ignition.

The instantaneous planar snapshots of temperature's distributions with the imposed spray are presented in Fig. 8. The observations of the spray allow to find differences indicated by the amount, size and temperature of the drops trapped in the reaction zone. The drop of the temperature around the the non reacting part of the jet, is also evident and is caused by the heat diffusion into the spray core. Clearly, observation of model E1 predictions, support the earlier conclusion about the rate in which the droplets evaporates which is slower than in E2 model. More so, a part highly heated droplets is convected further downstream thus elongating the flame, as was mentioned previously. This also makes the reaction zone thinner compared to model E2. Also in fig. 8 b) it can be observed that the heat diffusion to the droplets is most intense for that model, as the cooled zone in the vicinity of the tip of the reaction zone is most broad. In case of model E3 (Fig. 8 c)) the spray prevails almost across the whole flame zone. It is heated less intensely than in case of model E1 and hence more droplets are present inside the flame. For this model, as discussed previously the reaction zone is also the longest one. Noting the temperature distributions it can be stated that low heat diffusion rates into the bigger droplet in case of non-equilibrium model, led to the most broad high temperature zone.

Similar considerations but regarding the fuel distribution are given based on results in Fig. 9. Here the fuel distributions and the droplets are coloured by their diameters. Once again, model E2 clearly results in high concentration of rich fuel, very close to the reaction zone tip. Model E3 results in the highest spray penetration inside the flame, especially of the bigger drops. The characteristic feature of bigger droplets for all the models applied is that they radially dispersed from small droplets in the jet axis to bigger droplets away from the axis. What is not showed is that the smaller droplets follow well the flow velocity due to the fact that they are characterised by smaller Stokes numbers. The non-equilibrium effects are evident for E3 which allowed larger droplets to prevail further downstream. The influence of non-equilibrium effects for the smallest droplets is that they enhance the evaporation rates significantly (up to two times) [27]. Hence, one can observe that larger droplets are heated slower are convected downstream, while small droplets are already evaporated.

6 Conclusion and future work

Obtained results are followed by the conclusion that the choice of evaporation model in modelling the two phase reacting flows influenced the results but rather gently. The key parameter controlling the combustion process is in the evaporation rates predicted by each model. The "D^2 law" gives intermediate results in terms

of evaporation intensity and heat diffusion into the droplets comparing to the infinite conductivity model and the non-equilibrium model. The last one, is characterised by augmented evaporation rates especially in low temperature, but gives similar results compared to both remaining models. The non-equilibrium effects especially influence the smaller droplets what agree with the previous findings. Overprediction of temperatures is believed to be attributed to the global chemistry and this have significantly serious impact on results than chose between different evaporation models. This issue is attributed to further investigations. Even the discrepancies in the temperature profiles inside the reaction zones do not preclude the models from correct predictions the flames' lift-off heights in simulations with ILES approach on sufficiently dense meshes. It can be stated that for qualitative analysis of the two-phase reacting jet flames the use of each of evaporation model tested can lead to very similar results.

Acknowledgments

This work was supported by grant 2015/17/B/ST8/03217 (National Science Centre, Poland) and statutory funds BS/PB-1-103-3010/11/P. PL-Grid infrastructure was used to carry out the computations.

References

[1] W. O'Loughlin and A. R. Masri. A new burner for studying auto-ignition in turbulent dilute sprays. *Combust. Flame*, 158:1577–90, 2011.

[2] R. Cabra, T. Myhrvold, J.Y. Chen, A.N. Karpetis, R.W. Dibble, and R.S. Barlow. Lifted methane-air jet flames in a vitiated coflow. *Combust. Flame*, 143(4):491–506, 2005.

[3] W. Jones, A. Marquis, and K. Vogiatzaki. Large-eddy simulation of spray combustion in a gas turbine combustor. *Combust. Flame*, 161:222–39, 2014.

[4] A. Wawrzak and A. Tyliszczak. LES-CMC simulations of a turbulent hydrogen jet in oxy-combustion regimes. *Int. J. Hydrogen Energ.*, 41:9705–17, 2016.

[5] P. Schroll, A. P. Wandel, R. S. Cant, and E. Mastorakos. Direct numerical simulations of autoignition in turbulent two-phase flows. *Proc. Combust. Inst.*, 32(2):2275–82, 2009.

[6] V. N. Prasad, A. R. Masri, S. Navarro-Martinez, and K. H. Luo. Investigation of auto-ignition in turbulent methanol spray flames using large eddy simulation. *Combust. Flame*, 160:2941–94, 2013.

[7] C. Duwig, K. J. Nogenmyr, C. Chan, and M. J. Dunn. Large eddy simulations of a piloted lean premix jet flame using finite-rate chemistry. *Combustion Theory and Modelling*, 15:537–68, 2011.

[8] G. A. E. Godsave. Studies of the combustion of drops in a fuel spray: the burning of single drops of fuel. *Proc. Combust. Inst.*, pages 818–30, 1953.

[9] D. B. Spalding. The combustion of liquid fuels. *Proc. Combust. Inst.*, pages 847–64, 1953.

[10] B. Abramzon and W. A. Sirignano. Droplet vaporization model for spray combustion calculations. *Int. J. Heat Mass Transfer*, 32:1605–18, 1989.

[11] R. S. Miller, K. Harstad, and J. Bellan. Evaluation of equilibrium and non-equilibrium evaporation models for many-droplet gas-liquid flow simulations. *Int. J. Multiphase Flow*, 24:1025–55, 1998.

[12] J. Bellan and K. Harstad. Analysis of the convective evaporation of nondilute clusters of drops. *Int. J. Heat Mass Transfer*, 30:125–36, 1987.

[13] A Tyliszczak. High-order compact difference algorithm on half-staggered meshes for low mach number flows. *Comput. Fluids*, 127:131–45, 2016.

[14] A. Irannejad, A. Banaeizadeh, and F. Jaberi. Large eddy simulation of turbulent spray combustion. *Combust. Flame*, 162(2):431–50, 2015.

[15] W. Vreman. An eddy-viscosity subgrid-scale model for turbulent shear flow: Algebraic theory and applications. *Phys. Fluids*, 16:3670–81, 2004.

[16] H. Schmidt and U. Schumann. Coherent structure of the convective boundary layer derived from large eddy simulation. *J. Fluid Mech.*, 200:511–62, 1989.

[17] M.Maxey and J. Riley. Equation of motion for a small rigid sphere in a nonuniform flow. *Phys. Fluid*, 26:883–89, 1983.

[18] M. C. Yuen and L. W. Chen. On drag of evaporating liquid droplets. *Comb. Sci. Tech*, 14:147–54, 1976.

[19] R. Clift, J. R. Grace, and M. E. Weber. Bubbles, drops and particles. *New York: Academic Press*, 1978.

[20] J. O. Hirschfelder, C. F. Curtiss, and R. B. Bird. *Molecular Theory of Gases and Liquids*. John Wiley & Sons, Inc., New York, 1954.
[21] E. Fernandez-Tarrazo, A. L. Sanchez, and A. Linan. A simple one-step chemistry model for partially premixed hydrocarbon combustion. *Combust. Flame*, 147:32–7, 2006.
[22] Chakraborty N. A, E. Mastorakos, and R. S. Cant. Effects of turbulence on sprark ignition in inhomogeneous mmixture: a direct numerical simulation (DNS) study. *Comb. Sci. Tech*, 179(1-2):293–317, 2007.
[23] S.K. Lele. Compact finite difference with spectral-like resolution. *J. Comput. Phys.*, 103:16–42, 1992.
[24] A. Tyliszczak. A high-order compact difference algorithm for half-staggered grids for laminar and turbulent incompressible flows. *J. Comput. Phys.*, 276:438–67, 2014.
[25] L. Kuban, J. Stempka, A. Wawrzak, and A. Tyliszczak. DNS and ILES study of ethanol spray forced-ignition in a time-evolving mixing layer. *Proc. MCS 10*, 2017.
[26] A. Wawrzak and A. Tyliszczak. Implicit LES study of spark parameters impact on ignition in a temporally evolving mixing layer between H2/N2 mixture and air. *Int. J. Hydrogen Energ.*, (in press):1–14, 2018.
[27] D. Noh, S. Gallot-Lavallee, W. P. Jones, and S. Navarro-Martinez. Comparison of droplet evaporation models for a turbulent, non-swirling jet flame with a polydisperse droplet distribution. *Combust. Flame*, 194:135–51, 2018.
[28] P. Chassaing. *Turbulence en mecanique des fluides*. Cepadues-Editions, 2005.